NANO LETTERS

2008
Vol. 8, No. 4
1246-1252

Diameter Dependent Growth Rate and Interfacial Abruptness in Vapor–Liquid–Solid $Si/Si_{1-x}Ge_x$ Heterostructure Nanowires

Trevor E. Clark, Pramod Nimmatoori, Kok-Keong Lew,† Ling Pan,‡ Joan M. Redwing, and Elizabeth C. Dickey*

Department of Materials Science and Engineering and the Materials Research Institute, The Pennsylvania State University, University Park, Pennsylvania 16802

Received November 1, 2007; Revised Manuscript Received January 14, 2008

ABSTRACT

A strong diameter dependence is observed in the interfacial abruptness and growth rates in $Si/Si_{1-x}Ge_x$ axial heterostructure nanowires grown via Au-mediated low pressure CVD using silane and germane precursors. The growth of these nanowires has similarities to that of heterostructure thin films with similar compositional interfacial broadening, which increases with and is on the order with diameter. This broadening may reveal a fundamental challenge to fabrication of abrupt heterostructures via VLS growth.

$Si/Si_{1-x}Ge_x$ axial heterostructure nanowires (hNWs) have potential as components in electronic, photonic, and thermoelectric devices because of smaller device dimensions and performance enhancements from quantum confinement.[1,2] Successful implementation of these devices, however, requires being able to modulate the axial composition of the nanowires and form abrupt interfaces between segments.[3–7] For nanowires fabricated via the vapor–liquid–solid (VLS) growth mechanism, crystallization occurs from the liquid phase,[8] in which case the liquid-phase composition must be rapidly varied to grow axial heterostructures with chemically sharp interfaces between segments.

Thin-film counterparts to these $Si/Si_{1-x}Ge_x$ heterostructures, which are also pursued for improved performance relative to Si, have been difficult to fabricate with atomically abrupt interfaces because of Ge surface segregation during $Si_{1-x}Ge_x$ growth.[4–6,9–12] During thin-film fabrication via chemical vapor deposition (CVD) and molecular beam epitaxy (MBE), $Si_{1-x}Ge_x$ growth is initiated by adding a Ge source (e.g., GeH_4 or Ge) to a Si feed (e.g., SiH_4, $SiCl_4$, or Si). The Ge adatoms, however, segregate on the growth surface before being incorporated in the film because of the lower surface energy of Ge relative to Si. The segregated Ge must nearly saturate (≈90%) the surface before steady state $Si_{1-x}Ge_x$ films are grown.[13] The time required to saturate the surface depends on the Ge flux and results in nonabrupt leading $Si_{1-x}Ge_x$ interfaces with a shape approximated by an error function because the Ge composition must "build up" to an equilibrium value. This leading edge sharpens with increasing Ge composition because higher Ge fluxes yield shorter times to saturate the surface.[6,13] When the Ge source is turned off to resume growth of undoped Si, the nearly saturated surface acts as an unintentional Ge source and results in Ge incorporation in the Si cap. This yields a diffuse trailing interface, which is approximated by an exponential decay and results in thick (6–200 nm) regions of Ge in subsequent Si layers.[10,13,14] Even after growth of these unintentionally alloyed layers, the surface remains segregated with Ge.[6,10,13,14] Ge segregation can, however, be eliminated and abrupt interfaces fabricated by capping the surface during $Si_{1-x}Ge_x$ growth with atoms that saturate the dangling bonds (e.g., H or low energy surfactants like Ga, Sb, and As).[10] The former approach employing H is amenable to CVD in which a hydrogen containing precursor (e.g., SiH_4) or a H_2 carrier gas can be used.[10] The latter approach, although also effective in enabling abrupt interfacial growth, results in uncontrolled doping of the films because the surfactant is slowly incorporated in the growing film.[10]

Heterostructured nanowires, on the other hand, are usually grown via a different mechanism: VLS. Although it is not clear what role Ge segregation will play, if any, in attaining abrupt interfaces in $Si/Si_{1-x}Ge_x$ hNWs, it does seem clear that the mediating catalyst liquid can interfere with the ability

* Corresponding author. E-mail: ecd10@psu.edu.
† Current address: Power Electronic Branch, Naval Research Laboratory, Washington, DC 20375.
‡ Present address: Quality and Reliability, Logic Technology and Development, Intel Corporation, Hillsboro, Oregon 97124.

10.1021/nl072849k CCC: $40.75
Published on Web 03/06/2008

to vary the liquid-phase composition abruptly. This manuscript addresses these issues for hNWs grown via VLS.

Several groups have fabricated axial heterostructures of $Si/Si_{1-x}Ge_x$ and Si/Ge in nanowires via VLS.[15–19] Wu and co-workers used a hybrid of CVD ($SiCl_4$ precursor for Si) and pulse laser deposition (PLD) in which ablated Ge was periodically applied to the source stream.[15] The interfaces, however, were nonabrupt, with widths on the order of 40 nm for 200 nm diameter nanowires. The authors attribute the wide interfaces to slow gas-switching times. Redwing and co-workers fabricated $Si/Si_{1-x}Ge_x$ hNWs via low-pressure CVD with SiH_4 and GeH_4 precursors and also observed diffuse interfaces in 200 nm diameter hNWs.[16] Nonabrupt interfaces are also commonly observed in hNWs from III−V systems.[7,20–25] Only two groups have fabricated hNWs with atomically sharp interfaces via Au-mediated multiphase growth. The first used chemical beam epitaxy (CBE) to fabricate GaAs/InAs and InAs/InP hNWs and attributed the sharp interfaces to the high vapor pressure of the group V source materials, low growth rates (about 1 nm/s), and employment of growth interrupts between block switches.[21,24,25] There is also evidence, however, that these hNWs grow by a mechanism different to VLS: namely, a vapor−solid−solid (VSS) mechanism in which the seed particles remain solid during growth.[26] The same group has also fabricated abrupt interfaces in GaAsP/GaP hNWs via metal organic vapor-phase epitaxy (MOVPE).[23] They speculate that part of their success in this system stems from the low solubility of As in the catalyst. Another group has fabricated abrupt GaAsP/GaP hNWs via Au-mediated MBE.[27] These results from CBE, MOVPE, and MBE combined with the Ge segregation problems encountered in thin-film growth and the diffuse interfaces observed for hNWs beg the question as to whether or not fundamental impediments (like solute segregation) exist in obtaining abrupt interfaces via the VLS mechanism. In this paper, we address this question via an experimental study of $Si/Si_{1-x}Ge_x$ hNWs grown via gold-mediated VLS growth in a low-pressure (LP) CVD reactor.

We investigate the effect of diameter on the Ge compositional profiles and interfacial abruptness and also look for evidence of Ge segregation. Our results reveal that the interfacial properties of these hNWs are similar to those in thin films with similar leading and trailing edge broadening. This broadening appears to be caused by the time required to reestablish stable liquid catalyst compositions with feed vapor chemistry changes. The leading and trailing edges are also nonplanar, giving the $Si_{1-x}Ge_x$ segments a "capsule" shape, which we ascribe to coherency strains between the Si and $Si_{1-x}Ge_x$ segments. After growth of the $Si_{1-x}Ge_x$ segment, the catalyst appears to be a nonequilibrium Au−Si−Ge alloy and remains rich in Ge even after growth of a long (1 μm) Si-capping segment in a Ge-free feed. The abruptnesses of both edges are on the order of the hNW diameter, which is not predicted by expectations based on Ge segregation. The Si and $Si_{1-x}Ge_x$ growth rates are also measured as a function of diameter and observed to increase with diameter in a manner consistent with that predicted by the Gibbs–Thomson effect. Some of the ramifications of these results on axial doping of hNWs grown via VLS are also discussed.

$Si/Si_{1-x}Ge_x$ hNWs were grown via gold-mediated VLS growth in a LPCVD reactor at 500 °C and total pressure of 13 Torr. The deposition system[28] is equipped with a pressure-balanced vent-run manifold for the growth of multilayers. The hNWs are grown on an oxidized Si wafer coated with a thin (<2 nm) Au film in a 10% mixture of SiH_4 in H_2 and periodically admitted 2% mixture of GeH_4 in H_2.

The hNWs are composed of a long Si base grown for 6 min and six $Si_{1-x}Ge_x$ segments grown for 18 s each separated by Si segments also grown for 18 s. No growth interrupts are employed during application or removal of the GeH_4. The hNWs are terminated with a long Si segment grown for 60 s. The total gas flow rate is held constant at 400 sccm with a SiH_4 partial pressure of 590 mTorr and a GeH_4 partial pressure of 24 mTorr. These partial pressures yield a gas-phase Ge molar fraction (Ge/(Si + Ge)) of 4 atom % during GeH_4 introduction for which we expect a final Ge composition of ≈16 atom % in the $Si_{1-x}Ge_x$ segments based on single component $Si_{1-x}Ge_x$ NW growth.[29] Zhang and co-workers have shown, however, that the composition of homogeneous $Si_{1-x}Ge_x$ compound nanowires is diameter-dependent below ≈100 nm, with smaller wires being more rich in Si.[29] Hence, the composition of the $Si_{1-x}Ge_x$ segments in these hNWs is expected to have the same dependence with diameter. After growth, the hNWs were cooled to room temperature in an ambient of H_2 for approximately 30 min.

The hNWs were analyzed in two 200 kV JEOL TEMs: (1) a field-emission JEM 2010F, equipped with a scanning TEM (STEM) unit, high-angle annular dark-field (HAADF) detector, and energy dispersive spectrometer (EDS) and (2) a LaB_6-gun JEM 2010 equipped with a Gatan Tridiem energy filter. The HAADF-STEM images, EDS line profiles, and EDS maps were recorded with 1 or 0.2 nm probe sizes, although the STEM spatial resolution will be limited by beam broadening and is a maximum for the larger diameter wires, ≈1.3 nm for a 1 nm probe in a 40 nm diameter wire. Compositional profiles of the hNWs were obtained via intensity profiles of HAADF-STEM images. Energy-filtered Ge maps were acquired via the three-window background subtraction method of the Ge L edge at 1217 eV.[30] This method involves acquiring a set of three energy-filtered images by placing 50 eV windows around 1117 and 1177 eV for the pre-edge images employed for background subtraction and 1247 eV for the post-edge image. The acquisition time for each energy filtered image is 30 s.

For $Si/Si_{1-x}Ge_x$ hNWs, HAADF- or "Z-contrast" STEM is more efficient than EDS or EFTEM for collection of compositional maps. This is relevant not only from a collection-time standpoint, but also for minimization of beam damage. Employment of the HAADF-STEM technique, however, requires that the other contributions to image contrast be minimized so that the image intensity stems predominantly from atomic mass and not strain, which confounds intensity analysis,[31,32] especially for larger diameter (>40 nm) NWs. This is achieved by employing large

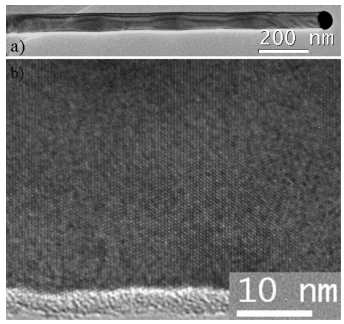

Figure 1. (a) Bright-field TEM image of a $Si/Si_{1-x}Ge_x$ hNW comprised of $Si_{1-x}Ge_x$ blocks separated by Si segments grown for the same duration. (b) HRTEM image of a $Si/Si_{1-x}Ge_x$ interface revealing the interfaces are coherent.

annular detector radii (>67 mrad) to minimize strain contrast. Analysis of larger diameters requires larger annular detector radii or conventional analytical (i.e., EDS or electron energy loss spectrometry) line profiles and elemental maps.

Most of the $Si/Si_{1-x}Ge_x$ hNWs from a single substrate and growth run have diameters between 8 and 40 nm; a small fraction (<1%) have diameters as large as 300 nm. A bright-field TEM image of a hNW supported by lacey carbon grown under similar conditions to those described above, but with segments grown for 9 s, is shown in Figure 1a.

The hNW is not tapered and has a ⟨111⟩ growth direction. The $Si_{1-x}Ge_x$ segments, which have higher average atomic mass, scatter electrons more effectively than the Si segments and are slightly darker in the image. Strain contrast between the segments arising from coherency strains is also evident in the bright-field image of Figure 1a. A HRTEM image of an interface between a Si and $Si_{1-x}Ge_x$ segment from another hNW (Figure 1b) reveals that the {111}-lattice fringes across the interface are continuous with no evidence of strain relaxation via formation of misfit dislocations. Hence, the interfaces are coherent. Figure 1b also reveals an oxide thickness of ≈5 nm on the wires. HRTEM of the rest of the hNW (not shown) reveals the oxide exists on both segments and does not vary in thickness along the length of the wire, indicating negligible uncatalyzed CVD deposition on the sidewalls during growth.

To study the Ge distribution in the hNWs, we employed HAADF-STEM as shown in Figure 2a. For thin specimens, intensity in these images varies approximately with the square of the average atomic number,[33,34] which enables one to observe compositional variations in both axial and radial directions. In Figure 2a, the Au catalyst particle is on the right. The hNW has a ⟨111⟩ growth direction and a 39 nm diameter, as measured in a Si segment before the leading edge of a $Si_{1-x}Ge_x$ segment.

Homogeneous compound $Si_{1-x}Ge_x$ NWs grown under similar conditions to those employed for growth of the $Si_{1-x}Ge_x$ segments but at 525 °C are tapered because of radial, thin-film growth and have rough surfaces.[28] In this work, however, the temperature has been reduced slightly (500 °C instead of 525 °C) and short growth durations (18 s) for the $Si_{1-x}Ge_x$ segments are employed. Higher magnification of the final four $Si_{1-x}Ge_x$ segments (Figure 2b,c)

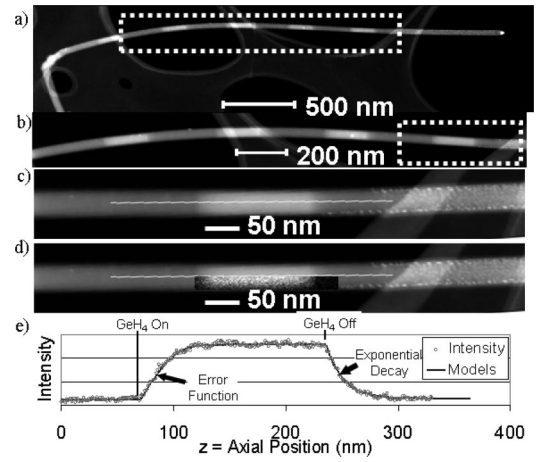

Figure 2. (a) Annular dark-field STEM image of a $Si/Si_{1-x}Ge_x$ hNW comprised of 6 $Si_{1-x}Ge_x$ blocks separated by Si segments grown for the same duration. The NW has a kink in the first $Si_{1-x}Ge_x$ segment. (b) Higher magnification ADF-STEM image revealing Si segments are longer than $Si_{1-x}Ge_x$. (c) Higher magnification ADF-STEM image of last $Si_{1-x}Ge_x$ segment revealing nonabruptness of interfaces. (d) ADF-STEM image with overlay of Ge EDS map revealing that HAADF image is dominated by atomic number contrast. (e) Intensity profile of last $Si_{1-x}Ge_x$ segment reveals asymmetric interfaces that are well-described by an error function (leading) and an exponential decay (trailing).

reveals the hNW has no appreciable $Si_{1-x}Ge_x$ thin-film growth.

Figure 2b also reveals that the $Si_{1-x}Ge_x$ segments are shorter than the Si segments, which confirms $Si_{1-x}Ge_x$ has a lower growth rate than Si at this composition[18] because the growth durations for the segments are the same. Measurements of the Si and $Si_{1-x}Ge_x$ growth rates of these hNWs are described below.

Figure 2c reveals that the capping segment is coated with small droplets having atomic mass heavier than Si. EDS (not shown) reveals the particles contain Au. These particles have been observed before during VLS growth of NWs and attributed to Au loss during thin-film growth,[28] Au diffusion during growth or cool-down,[35,36] or instabilities at the liquid−solid interface.[37] Our results, however, reveal that the Au loss is not occurring during thin-film growth because no thin-film growth is observed on any of the segments. In addition, the fact that the particles are only observed on the capping segment and not on the entire length reveals that the loss is not caused by instabilities during growth. Hence, we conclude that the Au loss is occurring after hNW growth (i.e., instabilities or surface diffusion after the SiH_4 is removed from the feed during cooling).

HAADF-STEM of the 39 nm hNW (Figure 2c) reveals that the leading ($Si-Si_{1-x}Ge_x$) and trailing ($Si_{1-x}Ge_x-Si$) interfaces have nonplanar shapes. This is confirmed via XEDS elemental mapping of Ge (overlaid in Figure 2d). The NW is damaged when the electron beam is stopped for the XEDS spot analyses required for the maps;[38] hence, this result is also confirmed via energy filtered TEM of another hNW (Figure 3). In this case, a broad beam and lower electron dose is employed. The HAADF-STEM images, XEDS map, and energy-filtered image also reveal that both

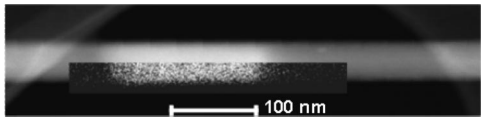

Figure 3. Annular dark-field STEM image of a Si/$Si_{1-x}Ge_x$ hNW with overlaid EFTEM Ge map revealing that curvature of trailing and leading interfaces is caused by variations in Ge composition.

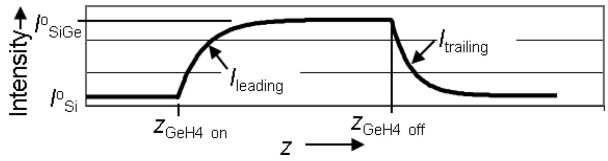

Figure 4. Schematic of intensity profile of asymmetric $Si_{1-x}Ge_x$ segment.

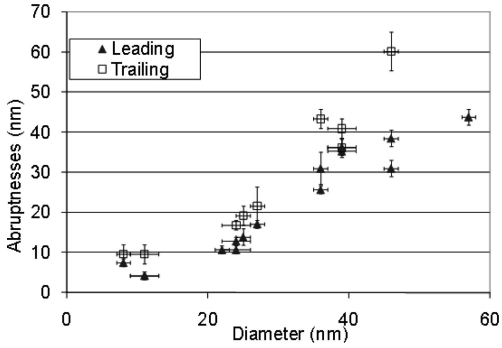

Figure 5. Abruptness of leading and trailing interfaces as a function of diameter for Si/$Si_{1-x}Ge_x$ hNWs.

the leading and trailing interfaces are diffuse. The intensity profile (Figure 2e) of a $Si_{1-x}Ge_x$ segment along the central growth axis reveals the compositional profiles are asymmetric. The leading edge can be modeled with an error function

$$I_{\text{leading}}(z) = (I^{\text{o}}_{\text{SiGe}} - I^{\text{o}}_{\text{Si}})\text{Erf}\left[\frac{z - z_{\text{GeH}_4\text{ on}}}{\lambda_{\text{leading}}}\right] + I^{\text{o}}_{\text{Si}} \qquad (1)$$

where I^o_{Si} is the average intensity from the Si block before GeH_4 is introduced to the feed, I^o_{SiGe} is the average intensity from the $Si_{1-x}Ge_x$ block after stabilization, z is the axial position, $Z_{GeH_4\ on}$ is the axial position of the onset of GeH_4 introduction, and $\lambda_{leading}$ is the characteristic distance of the interface, which is a fitting parameter. A schematic of the profile showing some of the model parameters is shown in Figure 4. We define the abruptness of the leading edge by the distance over which the intensity changes from 10% to 90% of the maximum value. It can be shown that, for an interface described by an error function, this distance ($z_{leading,90\%} - z_{leading,10\%}$) is 1.07 $\lambda_{leading}$. The intensity profiles of several hNWs of varying diameter are fit to the model and characteristic distances are determined. The corresponding abruptnesses, 1.07 $\lambda_{leading}$, are plotted in Figure 5, which reveals that the abruptness of the leading edge is approximately linearly dependent and on the same order as the diameter over the size range studied. The 35 nm hNWs have leading edge abruptnesses on the order of 25 nm and 10 nm hNWs have abruptnesses on the order of 5 nm.

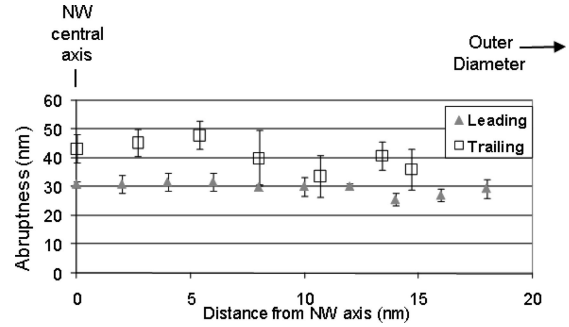

Figure 6. Abruptness of leading and trailing edges for a 36 nm hNW determined from intensity profiles at varying distance from the hNW axis.

The trailing edge, on the other hand, can be modeled by an exponential decay as shown in Figure 2e:

$$I_{\text{trailing}}(z) = (I^{\text{o}}_{\text{SiGe}} - I^{\text{o}}_{\text{Si}})\exp\left[\frac{z - z_{\text{GeH}_4\text{ off}}}{\lambda_{\text{trailing}}}\right] + I^{\text{o}}_{\text{Si}} \qquad (2)$$

where $Z_{GeH_4\ off}$ is the axial position of the onset of GeH_4 removal from the feed and $\lambda_{trailing}$ is the characteristic distance of the trailing interface, which is also a fitting parameter. In an analogous approach to that used for the leading edge, we define the abruptness of the trailing edge by the distance over which the intensity decays from 90% to 10%. It can be shown that, for an exponential decay, this distance ($z_{leading,10\%} - z_{leading,90\%}$) is 2.41 $\lambda_{trailing}$. The abruptness of the trailing edge also varies roughly linearly with diameter, as shown in Figure 5. Comparison of the leading and trailing abruptness reveals that the leading edge is more abrupt than the trailing edge, which is consistent with the observations from thin-film growth.[6,12,13,39]

The capsule shape of the $Si_{1-x}Ge_x$ segments (Figures 2d and 3) actually confounds our determination of the true interfacial width because of the signal collection from the entire hNW thickness inherent to TEM. This projection effect will cause the interfaces to appear broader than they actually are and will be strongest along the axis; hence the interfacial widths measured along the axis, as is the case in this study, will be overestimated. To determine the extent of this effect, we measured the interface abruptness from intensity profiles taken at different distances from the axis for one of the larger (36 nm) hNWs (not shown). (Because the coherency strain increases with increasing diameter, the interfacial nonplanarity is largest for larger diameter hNWs.) The results (Figure 6) reveal that the widths of both interfaces when acquired from the axial intensity profile are not inflated by the projection effect. Hence the diameter dependence observed in Figure 5 is not an artifact from the projection effect.

The diffuseness and asymmetry of the leading and trailing interfaces appear to be analogous to those observed in thin-film Si/$Si_{1-x}Ge_x$ heterostructures. Because any Ge at the hNW growth front may have detrimental effects on our ability to modulate the composition of the hNWs, we looked for evidence of Ge at the interface of the capping Si segment and the catalyst particle. EDS of the Au catalyst particle (Figure 7) and an EDS line profile of the end of the capping Si segment and catalyst (Figure 8) reveal that Ge remains in the catalyst longer than 1 min after the GeH_4 is removed

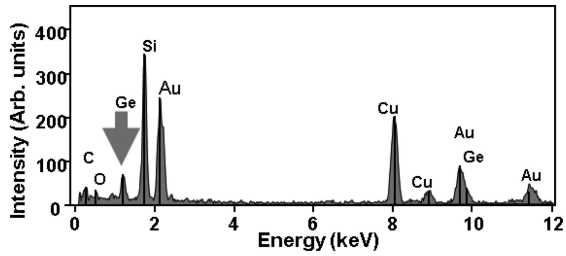

Figure 7. EDS spectrum of the catalyst particle reveals Ge 1 min after GeH_4 has been removed from the feed. The Cu peak is an artifact from the support grid, which is heavily fluoresced from the Au L_{α_1} X-rays.

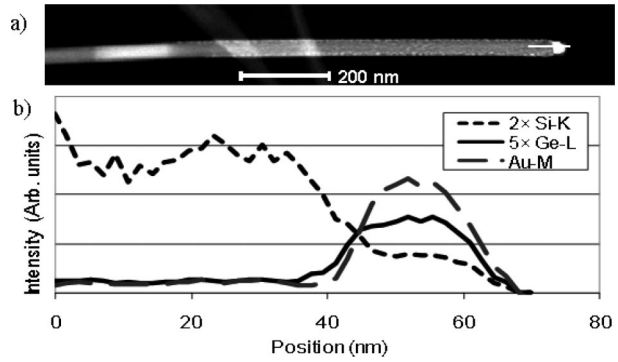

Figure 8. (a) ADF-STEM image of capping Si segment and catalyst particle, (b) EDS line profile of capping segment and catalyst particle.

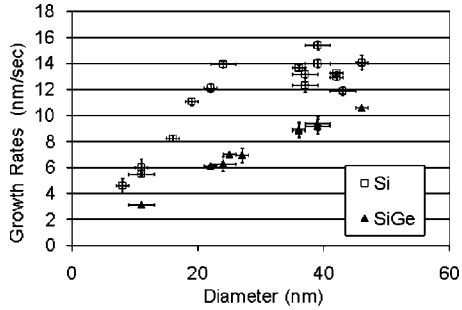

Figure 9. Si and $Si_{1-x}Ge_x$ growth rates determined from measurements of the segment lengths.

from the feed; during this time, 800 nm of Si (perhaps alloyed with Ge) is grown. (The Cu peak in the EDS spectrum is an artifact from the support grid, which is heavily fluoresced from the Au L_{α_1} X-rays.) Ge is detected in catalyst particles from other hNWs with larger and smaller diameters as well. We attempted to detect unintentional Ge alloying in the capping Si segment via EDS, but the Ge is below the detectable limit (≈0.8 atom %).[29]

The EDS line profile (Figure 8b) confirms Ge exists through the entire volume of the catalyst particle and is not just segregated at the Si−catalyst interface, which demonstrates that under these conditions the composition of the liquid catalyst is not being fully depleted of Ge, at least on the minute time scale.

The intensity profiles (e.g., Figure 2e) also enable determination of the lengths of Si and $Si_{1-x}Ge_x$ segments grown during application of (1) SiH_4 and (2) SiH_4 and GeH_4 because the onsets for GeH_4 incorporation, $Z_{GeH_4\ on}$, and GeH_4 removal, $Z_{GeH_4\ off}$, are well-defined (Figure 4). The $Si_{1-x}Ge_x$ growth rate, $\dot{L}_{SiGe}$, can then be calculated

$$\dot{L}_{SiGe} = \frac{z_{GeH_4\ off} - z_{GeH_4\ on}}{18\ s} \quad (3)$$

We have assumed that the instantaneous growth rate of the $Si_{1-x}Ge_x$ segment is independent of Ge composition. The Si growth rate can be obtained in an analogous manner. A plot of the Si and $Si_{1-x}Ge_x$ growth rates as a function of diameter is shown in Figure 9. We have included the growth of the leading interface in the $Si_{1-x}Ge_x$ segment length and the growth of the trailing edge in the Si segment length; hence, there is some error in the determinations. At large diameters, this error would be largest because the interfaces are more diffuse, which would tend to cause underestimations in the growth rates. Thus the growth-rate dependence, if anything, is underestimated in this plot. Nevertheless, Figure 9 reveals a diameter-dependence to the growth rates for diameters less than 30 nm for Si and less than 50 nm for $Si_{1-x}Ge_x$. Interpretation of the $Si_{1-x}Ge_x$ growth rate is complicated by the fact that the composition is also size dependent in these $Si_{1-x}Ge_x$ segments.[29]

These trends appear to confirm the expectation of size-dependent growth rates based on the Gibbs–Thomson effect. Whereas in VLS-grown Si nanowires from $SiCl_4$, both decreasing and increasing growth rates as a function of nanowire diameter have been observed,[15,40–43] prior work using Si_2H_6 precursors have shown an invariant behavior.[44] Schmidt et al. provided a consistent interpretation of all of these behaviors by taking into consideration both the incorporation of Si into the catalyst and the crystallization step.[43] In this model, when the reactive sticking coefficient is independent of the Si chemical potential in the catalyst droplet, the growth velocity does not depend on the wire diameter, which is consistent with the Kodabama et al. results and interpretation.[44] Our work differs from this previous work[44] in a few ways. First, growth in the present study is carried out with SiH_4 and at much higher pressures than those employed in the prior studies using Si_2H_6 (13 Torr compared to 10^{-6} Torr in ref 44). Second, tapering due to Au loss from the nanowire during growth is not observed in our experiments. Lastly, the size regime of our nanowires is much smaller; the lower bounds studied by Kodabama et al. is 50 nm, where our work addresses nanowires smaller than 50 nm where size effects are more likely. Our observed diameter-dependent growth rates with a SiH_4 precursor reveal that either the reactive sticking coefficient or Si evaporation rate does depend on the Si chemical potential in the droplet, at least in certain growth regimes (e.g., high pressures), thus leading to size-dependent growth rates even with SiH_4 precursors.

Referring back to Figure 9, the trends also reveal that the size dependence persists in the presence of GeH_4. The higher growth rate of Si relative to $Si_{1-x}Ge_x$ persists over the entire diameter range for these compositions. These results also confirm that there is a minimum diameter (8 nm for Si) below which we expect no growth; the critical diameter for Si is consistent with that observed for single component Si NWs (≈2 nm) grown via atmospheric pressure CVD at temperatures between 365 and 495 °C.[45]

Our hypothesis for the cause of the diffuse interfaces (Figure 2d,e) is that there is a delay between the modulation times for the vapor and liquid phases. This delay is caused by the time required to establish a steady-state composition of the liquid phase, which involves not only incorporation of new solute atoms (e.g., Ge for the formation of $Si_{1-x}Ge_x$ segments) but also expulsion of the excess solute atoms (e.g., Si for the formation of $Si_{1-x}Ge_x$ segments) either by evaporation into the vapor phase or by incorporation in the growing hNW. The latter (incorporation) leads to broadening of both leading and trailing interfaces.[46] Although a model that predicts the shape of the profiles based on the incorporation process has been developed,[46] the linear dependence of the trailing edge broadening with the diameter is expected if one considers the time required to reestablish a stable catalyst composition. This time will scale with the quotient of the number of atoms in the catalyst (proportional to the catalyst volume d^3) and the area of the catalyst−hNW interface (proportional to d^2). Here we have assumed that the depletion of any excess atoms in the catalyst occurs predominantly via incorporation into the hNW through the catalyst−hNW interface.

Hence, the length of NW grown during this transition time is proportional to the diameter, which is consistent with the variation in abruptness observed for these hNWs (Figure 5). More abrupt interfaces may be attainable by employing a catalyst with a lower solubility of Ge and Si (e.g., solid Al), as suggested in refs 46, 47. In fact, the abrupt interfaces observed in growth of III−V axial hNWS are believed to be possible because of the employment of a solid catalyst with a low solubility.[21,24–26] Our results suggest similar challenges exist in $Si/Si_{1-x}Ge_x$ hNW formation and that perhaps similar approaches to those employed to form abrupt III−V hNWs (i.e., solid catalysts, low growth rates, growth interrupts) are necessary to form abrupt interfaces in this system as well.

Besides nonabrupt interfaces, another ramification of this hypothesis is that the first leading edge will be broader than the subsequent leading edges because the catalyst is initially devoid of any Ge and hence it must take longer to saturate it and the transition will be longer.

Our results reveal that, under these growth conditions, the interfaces of the $Si_{1-x}Ge_x$ segments are not only diffuse but nonplanar (Figures 2d and 3). We hypothesize that the curvature of the interfaces is caused by strain from the coherent $Si_{1-x}Ge_x$ segments on the Si segments (Figure 1b). Roper and co-workers have developed a model to predict the effect of growth on the curvature of the growth front of single component Si NWs grown via Au-mediated VLS.[48] Their model predicts that the growth front will curve 44° from the horizontal. The anisotropy of the crystalline NW, however, is not included in their consideration. In our case, however, we observe both concave and convex interfacial shapes, which is not predicted by their model. Hence, we suspect the nonplanarity is not necessarily caused by a nonplanar growth front but by strain.

The growth of $Si/Si_{1-x}Ge_x$ hNWs via Au-mediated CVD is similar to that in thin films with similar leading and trailing edge broadening and that a source (i.e., the catalyst) must be saturated prior to stable growth. The catalyst particle remains rich in Ge even after Ge is removed from the feed and reveals that the catalyst is not being fully depleted of Ge in keeping with the vapor phase composition. It is not clear whether this will impede subsequent growth of unalloyed Si segments. The leading and trailing edges of the $Si_{1-x}Ge_x$ segments are parabolic, giving the $Si_{1-x}Ge_x$ segments a "capsule" shape. The curvature of the interfaces is likely caused by strain from the coherent $Si_{1-x}Ge_x$ segments on the Si segments. The diffuse interfaces, which increase in width with increasing diameter, may reveal a fundamental impediment to formation of chemically abrupt interfaces via the vapor–liquid–solid (VLS) mechanism. The diameter dependence can be predicted based on the time required to restabilize the liquid catalyst composition. It is conceivable that this broadening may be reduced or eliminated if a catalyst with a lower Ge solubility is employed. The growth rates of both the Si and $Si_{1-x}Ge_x$ also have a diameter dependence consistent with previous observations. Si growth has a critical diameter less than 8 nm, also consistent with previous observations.

Acknowledgment. Discussions and correspondence with Na Li and Teh Tan at Duke University and Peter Voorhees and Steven Roper at Northwestern University are acknowledged. This publication was supported by the MRSEC for Nanoscale Science (DMR-0213623), NIRT (ECS 06-09282), and the Pennsylvania State University Materials Research Institute NanoFabrication Network and the National Science Foundation Cooperative Agreement no. 0335765, National Nanotechnology Infrastructure Network, with Cornell University.

References

(1) Li, D. Y.; Wu, Y.; Fan, R.; Yang, P. D.; Majumdar, A. *Appl. Phys. Lett.* **2003**, *83*, 3186–3188.
(2) Björk, M. T.; Thelander, C.; Hansen, A. E.; Jensen, L. E.; Larsson, M. W.; Wallenberg, L. R.; Samuelson, L. *Nano Lett.* **2004**, *4*, 1621–1625.
(3) Berbezier, I.; Ronda, A.; Portavoce, A. *J. Phys.: Condens. Matter* **2002**, *14*, 8283–8331.
(4) Benedetti, A.; Norris, D. J.; Hetherington, C. J. D.; Cullis, A. G.; Armigliato, A.; Balboni, R.; Robbins, D. J.; Wallis, D. J. *Microscopy of Semiconducting Materials 1999*; Institute of Physics Conference Series, Number 164; Institute of Physics Publishing: Philadelphia, 1999; pp 219−222.
(5) Benedetti, A.; Norris, D. J.; Hetherington, C. J. D.; Cullis, A. G.; Robbins, D. J.; Wallis, D. *J. Appl. Phys.* **2003**, *93*, 3893–3899.
(6) Jernigan, G. G.; Thompson, P. E.; Silvestre, C. L. *Surf. Sci.* **1997**, *380*, 417–426.
(7) Borgström, M. T.; Verheijen, M. A.; Immink, G.; de Smet, T.; Bakkers, E. *Nanotechnology* **2006**, *17*, 4010–4013.
(8) Wagner, R. VLS Mechanism of Crystal Growth. In *Whisker Technology*; Levitt, A., Ed.; Wiley: New York, 1970; pp 47–119..
(9) Godbey, D. J.; Ancona, M. G. *J. Vac. Sci. Technol., A* **1997**, *15*, 976–980.
(10) Grutzmacher, D. A.; Sedgwick, T. O.; Powell, A.; Tejwani, M.; Iyer, S. S.; Cotte, J.; Cardone, F. *Appl. Phys. Lett.* **1993**, *63*, 2531–2533.
(11) Walther, T.; Humphreys, C. *J. Cryst. Growth* **1999**, *197*, 113–128.
(12) Norris, D. J.; Cullis, A. G.; Grasby, T. J.; Parker, E. H. C. *J. Appl. Phys.* **1999**, *86*, 7183–7185.
(13) Godbey, D. J.; Ancona, M. G. *J. Vac. Sci. Technol., B* **1993**, *11*, 1120–1123.
(14) Tok, E. S.; Woods, N. J.; Zhang, J. *J. Cryst. Growth* **2000**, *209*, 321–326.
(15) Wu, Y. Y.; Fan, R.; Yang, P. D. *Nano Lett.* **2002**, *2*, 83–86.

(16) Redwing, J. M.; Lew, K.-K.; Bogart, T.; Pan, L.; Dickey, E. C.; Carim, A. H.; Wang, Y.; Cabassi, M.; Mayer, T. S. *Proc. SPIE-Int. Soc. Opt. Eng.* **2004**, *5361*, 52.
(17) Dujardin, R.; Poydenot, V.; Devillers, T.; Favre-Nicolin, V.; Gentile, P.; Barski, A. *Appl. Phys. Lett.* **2006**, *89*, 153129.
(18) Zakharov, N. D.; Werner, P.; Gerth, G.; Schubert, L.; Sokolov, L.; Gösele, U. *J. Cryst. Growth* **2006**, *290*, 6–10.
(19) Hanke, M.; Eisenschmidt, C.; Werner, P.; Zakharov, N. D.; Syrowatka, F.; Heyroth, F.; Schafer, P.; Konovalov, O. *Phys. Rev. B* **2007**, *75*, 161303.
(20) Hiruma, K.; Murakoshi, H.; Yazawa, M.; Katsuyama, T. *J. Cryst. Growth* **1996**, *163*, 226–231.
(21) Ohlsson, B. J.; Björk, M. T.; Persson, A. I.; Thelander, C.; Wallenberg, L. R.; Magnusson, M. H.; Deppert, K.; Samuelson, L. *Physica E* **2002**, *13*, 1126–1130.
(22) Gudiksen, M. S.; Lauhon, L. J.; Wang, J.; Smith, D. C.; Lieber, C. M. *Nature* **2002**, *415*, 617–620.
(23) Seifert, W.; Borgström, M.; Deppert, K.; Dick, K. A.; Johansson, J.; Larsson, M. W.; Martensson, T.; Skold, N.; Svensson, C. P. T.; Wacaser, B. A.; Wallenberg, L. R.; Samuelson, L. *J. Cryst. Growth* **2004**, *272*, 211–220.
(24) Björk, M. T.; Ohlsson, B. J.; Sass, T.; Persson, A. I.; Thelander, C.; Magnusson, M. H.; Deppert, K.; Wallenberg, L. R.; Samuelson, L. *Appl. Phys. Lett.* **2002**, *80*, 1058–1060.
(25) Samuelson, L.; Thelander, C.; Björk, M. T.; Börgstrom, M.; Deppert, K.; Dick, K. A.; Hansen, A. E.; Martensson, T.; Panev, N.; Persson, A. I.; Seifert, W.; Skold, N.; Larsson, M. W.; Wallenberg, L. R. *Physica E* **2004**, *25*, 313–318.
(26) Persson, A. I.; Larsson, M. W.; Stenstrom, S.; Ohlsson, B. J.; Samuelson, L.; Wallenberg, L. R. *Nat. Mater.* **2004**, *3*, 677–681.
(27) Chen, C.; Plante, M. C.; Fradin, C.; LaPierre, R. R. *J. Mater. Res.* **2006**, *21*, 2801–2809.
(28) Lew, K.-K.; Pan, L.; Dickey, E. C.; Redwing, J. M. *J. Mater. Res.* **2006**, *21*, 2876–2881.
(29) Zhang, X.; Lew, K.-K.; Nimmatoori, P.; Redwing, J. M.; Dickey, E. C. *Nano Lett.* **2007**, *7*, 3241–3245.
(30) Egerton, R. In *Electron Energy Loss Spectroscopy in the Electron Microscope*; Plenum: New York, 1986; pp 304 and 331.
(31) Walther, T.; Humphreys, C. J. *Electron Microscopy and Analysis 1997*; Institute of Physics Conference Series, Number 153; Institute of Physics Publishing: Philadelphia, 1997; pp 303−306.
(32) Williams, D. B.; Carter, C. B. *Transmission Electron Microscopy*; Plenum Press: New York, 1996; p 359.
(33) Pennycook, S. J.; Boatner, L. A. *Nature* **1988**, *336*, 565–567.
(34) Browning, N. D.; Chisholm, M. F.; Pennycook, S. J. *Nature* **1993**, *366*, 143.
(35) Hannon, J. B.; Kodambaka, S.; Ross, F. M.; Tromp, R. M. *Nature* **2006**, *440*, 69–71.
(36) Kodambaka, S.; Hannon, J. B.; Tromp, R. M.; Ross, F. M. *Nano Lett.* **2006**, *6*, 1292–1296.
(37) Pan, L.; Lew, K.-K.; Redwing, J. M.; Dickey, E. C. *J. Cryst. Growth* **2005**, *277*, 428–436.
(38) Bell, D. C.; Wu, Y.; Barrelet, C. J.; Gradecak, S.; Xiang, J.; Timko, B. P.; Lieber, C. M. *Microsc. Res. Tech.* **2004**, *64*, 373–389.
(39) Walther, T.; Humphreys, C. J.; Robbins, D. J. *Defect Diffus. Forum* **1997**, *143*, 1135–1140.
(40) Givargizov, E. I. *J. Cryst. Growth* **1975**, *31*, 20–30.
(41) Nebol'sin, V. A.; Shchetinin, A. A.; Dolgachev, A. A.; Korneeva, V. V. *Inorg. Mater.* **2005**, *41*, 1256–1259.
(42) Weyher, J. *J. Cryst. Growth* **1978**, *43*, 235–244.
(43) Schmidt, V.; Senz, S.; Gösele, U. *Phys. Rev. B* **2007**, *75*, 045335.
(44) Kodambaka, S.; Tersoff, J.; Reuter, M.; Ross, F. M. *Phys. Rev. Lett.* **2006**, *96*, 1–4.
(45) Kikkawa, J.; Ohno, Y.; Takeda, S. *Appl. Phys. Lett.* **2005**, *86*, 123109.
(46) Li, N.; Tan, T.; Gösele, U. *J. Appl. Phys. A: Mater. Sci. Process.* **2008**, *90*, 591–596.
(47) Wang, Y. W.; Schmidt, V.; Senz, S.; Gösele, U. *Nat. Nanotechnol.* **2006**, *1*, 186–189.
(48) Roper, S. M.; Davis, S. H.; Norris, S. A.; Golovin, A. A.; Voorhees, P. W.; Weiss, M. *J. Appl. Phys.* **2007**, *102*, 1–7.

NL072849K